Organometallic conjugates of the drug sulfadoxine for combatting antimicrobial resistance

Chellan, P.; Duffy, A. S.; Triccas, J. A.; Tam, C.; Cheng, L. W. ; Liu, J.; Land, K. M. ; Clarkson, G. J. ; Romero Canelon, Isolda; Sadler, P. J.

DOI:
10.1002/chem.201801090

CHEMISTRY
A European Journal

A Journal of
ChemPubSoc Europe

Accepted Article

Title: Organometallic conjugates of the drug sulfadoxine for combatting antimicrobial resistance

Authors: Peter J. Sadler, Prinessa Chellan, Vicky Avery, Sandra Duffy, James Triccas, Gayathri Nagalingam, Christina Tam, Luisa Cheng, Jenny Liu, Kirkwood Land, Guy Clarkson, and Isolda Romero

To be cited as: *Chem. Eur. J.* 10.1002/chem.201801090

Link to VoR: http://dx.doi.org/10.1002/chem.201801090

Supported by
ACES

WILEY-VCH

10.1002/chem.201801090

WILEY-VCH

FULL PAPER

Organometallic conjugates of the drug sulfadoxine for combatting antimicrobial resistance

Prinessa Chellan,[a],†,* Vicky M Avery,[b] Sandra Duffy, [b] James A. Triccas,[c] Gayathri Nagalingam,[c] Christina Tam, [d] Luisa W. Cheng, [d] Jenny Liu,[e] Kirkwood M. Land,[e] Guy J. Clarkson,[a] Isolda Romero-Canelón,[a] Peter J. Sadler*,[a]

Abstract: Fourteen novel arene Ru^{II}, and cyclopentadienyl (Cp^x) Rh^{III} and Ir^{III} complexes containing an *N,N'*-chelated pyridylimino- or quinolylimino ligand functionalized with the antimalarial drug sulfadoxine have been synthesized and characterized, including three by x-ray crystallography. The rhodium and iridium complexes exhibited potent antiplasmodial activity with IC_{50} values of 0.10 – 2.0 μM in either all, or one of the three *Plasmodium falciparum* assays (3D7 chloroquine sensitive, Dd2 chloroquine resistant and NF54 sexual late stage gametocytes) but were only moderately active towards *Trichomonas vaginalis*. They were active in both the asexual blood stage and the sexual late stage gametocyte assays, whereas the clinical parent drug, sulfadoxine, was inactive. Five complexes were moderately active against *Mycobacterium tuberculosis* (IC_{50} < 6.3 μM), while sulfadoxine showed no antitubercular activity. An increase in the size of both the Cp^x ligand and the aromatic imino substituent increased hydrophobicity, which resulted in an increase in antiplasmodial activity.

Introduction

Infectious diseases remain the leading cause of morbidity and mortality in Sub-Saharan Africa with *Mycobacterium tuberculosis*, HIV/AIDS and malaria remaining the biggest killers.[1] In 2015, an estimated 1.8 million people died from TB infection, an appallingly high number since it is preventable. The HIV/AIDS epidemic and the emergence of multidrug resistant *M. tuberculosis* has made development of novel drug therapies a pressing task. According to the World Health Organisation, people living with HIV are ≈ 26-31 times more likely to develop TB compared to healthy individuals, and 35 % of HIV deaths reported was a result of TB infection, making it the primary killer of HIV-positive individuals.[2] An added complication for these same individuals is their exposure to parasitic diseases, such as malaria. An estimated 212 million cases and 429,000 deaths occurred in 2015, as a result of malaria caused by *Plasmodium falciparum* infection.[3] Currently, the standard first line therapy for uncomplicated *P. falciparum* malaria infections is artemisinin-based combined therapy (ACT).[4, 5]

ACT is a combination of artemisinin or an artemisinin derivative and a partner drug with a separate parasite target (and longer in vivo half-life) in order to increase efficacy and decrease the risk of development of resistance. As well as TB, resistance of *P. falciparum* to all drugs inclusive of artemisinin and its derivatives, has been reported in several parts of Asia.[6, 7] The majority of new drug candidates for both TB and malaria currently in development are organic analogues of previously used clinical drugs, or specifically for malaria, novel chemistry clustering into only a handful of novel drug targets such as PI4K,[8] and ATP4.[9] The application of metal-containing compounds for the treatment of parasitic diseases has emerged as a vital area of research. Taking advantage of the redox potential of metals, new multi-targeting drugs can be designed that can kill the parasite through induction of oxidative stress.[10-12] A common strategy in drug discovery today is the 'repurposing' and/or derivatization of drugs used for treatment of other illnesses to identify new candidates that can be taken to clinical trials more rapidly than completely novel drugs.[13, 14] With this strategy in mind, it is possible to design new metallo-therapeutics through conjugation of a drug derivative and bioactive metal fragments. In the last decade, the study of metallo-therapeutics as potential anti-parasitics has gained momentum.[15-20] In particular, the discovery of the potent activity of ferroquine,[21-23] a ferrocene-chloroquine conjugate, has encouraged the design of novel metal complexes containing validated drug scaffolds.[4, 24]

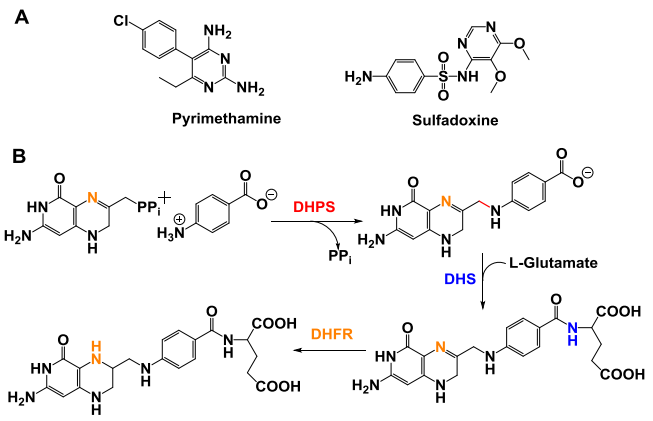

Figure 1. A) Structures of pyrimethamine and sulfadoxine; B) Parasitic folate synthetic pathway.[25]

[a] Department of Chemistry, University of Warwick, Coventry, CV4 7AL, UK
[b] Discovery Biology, Griffith Institute for Drug Discovery, Griffith University, Nathan, Queensland 4111, Australia
[c] Microbial Immunity and Pathogenesis Group, Department of Infectious Diseases and Immunology, Sydney Medical School, The University of Sydney, Sydney, NSW 2006, Australia
[d] Foodborne Toxin Detection and Prevention Research Unit, Agricultural Research Service, United States Department of Agriculture, Albany, CA 94710
[e] Department of Biological Sciences, University of the Pacific, Stockton, CA 95211
* Corresponding Authors: email: p.j.sadler@warwick.ac.uk, +4424 7652 3818; p.chellan@sun.ac.za, +27218083327
† Current address: Stellenbosch University, Matieland, Western Cape, South Africa
Supporting information for this article is available on the WWW under http://dx.doi.org/10.1002/chem.2018xxxxx. CCDC 1503886-1503888 contains the crystallographic data for **this article**, in CIF format. These data can be obtained free of charge at www.ccdc.cam.ac.uk/conts/retrieving.html [or from the Cambridge Crystallographic Data Centre, 12, Union Road, Cambridge CB2 1EZ, UK; fax: (internat.) +44-1223/336-033; E-mail: deposit@ccdc.cam.ac.uk].

Sulfadoxine is a drug belonging to the class known as sulfonamides and is used in combination with pyrimethamine (Figure 1A) to treat malaria caused by the *P. falciparum* parasite. Pyrimethamine and sulfadoxine target two enzymes that are crucial to the parasitic folate biosynthetic pathway, i.e. dihydrofolate reductase (DHFR) and dihydropteroate synthetase (DHPS), Figure 1B.[25] DHFR has been validated as a clinical target for several illnesses and protozoan DHFR has been shown to be structurally different from the mammalian enzyme.[26] This could have relevance for the selectivity of new inhibitors prepared from sulfadoxine or pyrimethamine.

Sulfonamides have been used to treat microbial and parasitic infections.[27] Cobalt, copper, nickel and zinc complexes of the sulfonamide, 4-{[(E)-(5-bromo-2-hydroxyphenyl)methylidene]-amino}-N-(4,6-dimethyl-pyrimidin-2-yl)benzenesulfonamide, have shown moderate to significant antibacterial activity against one or more bacterial strains and good antifungal activity against various fungal strains.[28] A library of complexes prepared from (5-chloro-2-hydroxybenzylidene)aminobenzenesulfonamides with the general formula $[L_2(M)_2H_2O]$ (where M is Co, Cu, Zn, Ni or Mn) were able to reduce epimastigote proliferation and were cidal for trypomastigotes of *Trypanosoma cruzi* Y strain.[29]

Here we have synthesized new half-sandwich organo-ruthenium(II), -rhodium(III) and -iridium(III) complexes containing chelated pyridyl- or quinolyl-imino ligands derivatized with the drug sulfadoxine and screened them for *in vitro* biological activity against various parasite strains and *Mycobacterium tuberculosis*. Remarkably, the conjugation to organometallic fragments switched on the activity of sulfadoxine towards several strains of microorganisms and the malaria parasite, towards which the clinical drugs, pyrimethamine and chloroquine were also inactive.

Results and Discussion

Synthesis. The two new Schiff base ligands, *N*-(5,6-di-methoxypyrimidin-4-yl)-4-((pyridin-2-ylmethylene)amino)-benzenesulfonamide (2-pyridyliminesulfadoxine, **L1**) and *N*-(5,6-dimethoxypyrimidin-4-yl)-4-((isoquinolin-3-ylmethylene)amino)-benzenesulfonamide (2-quinolyliminesulfadoxine, **L2**) were synthesised using a microwave method (**Scheme 1**) and isolated as crude beige and yellow solids, respectively. Attempts to purify **L1** and **L2** were unsuccessful and they were used in subsequent reactions without further purification.

New organometallic conjugates of the clinical antimicrobial drug sulfadoxine were synthesised by reaction of **L1** and **L2** with the appropriate ruthenium(II) arene, and rhodium(III) or iridium(III) cyclopentadienyl chloride dimers in methanol over 16 h. Treatment with ammonium hexafluorophosphate yielded fourteen novel cationic *N,N'*-chelated complexes (**1**-**14**) (**Scheme 2**) as microcrystalline yellow or orange solids. Complexes **1**-**14** were characterised by 1D and 2D NMR, ESI-MS, and elemental analysis, and for the complexes **2**, **10** and **13**, by single crystal X-ray diffraction. The purity of the complexes was confirmed using RP-HPLC.

The amino (NH) proton of the sulfonamide moiety was observed as a broad singlet downfield in the ^{1}H NMR spectra for all complexes between 9.87 – 10.00 ppm (see Supporting Information). For the rhodium pyridyl complexes (**2**-**4**), this resonance was slightly upfield (δ 9.05-9.10 ppm) compared to the quinolylimino sulfadoxine analogues (**9**-**11**; δ 9.10-9.45 ppm). Similar differences are notable for the iridium derivatives (**5**-**7** and **12**-**14**). In the Rh and Ir complexes with either the Cp^{*ph} (**3**, **4**, **10**, **11**) or Cp^{*biph} (**6**, **7**, **13**, **14**) ligands, the extended aromatic Cp^x ligand gave rise to increased shielding of the aromatic proton adjacent to the pyridyl or quinolyl nitrogen compared to the corresponding Cp* derivative (**2**, **7**, **9** and **12**). Similar resonances were observed for the arene/Cp^x ancillary ligands in all complexes. High resolution positive-ion ESI-MS confirmed the identity of the complexes, with a base peak corresponding to the cationic molecular ($[M]^+$ - PF_6^-) ion for all complexes. HPLC analysis confirmed the purity of complexes **1**-**14**, each displaying two peaks, one for the chloride complex and the other for the aqua complex. Though the samples were freshly prepared prior to injection in water-acetonitrile, displacement of the chloride ligand by water for a proportion of each complex occurred during the course of the HPLC analysis.

The molecular structures of complexes **2**, **10** and **13** (Figures 2 - 4) were determined using X-ray diffraction. Crystals were grown by slow evaporation of a mixture of acetone-diethyl ether at ambient temperature. Tables S1 and S2 in the Supporting Information lists the crystallographic data and short contact distances for **2**, **10** and **13**. Table 1 shows selected bond lengths and angles for each structure.

All of the complexes crystallised in a triclinic system and P-1 space group. The crystals of **10** and **13** are isomorphic and isostructural; with two molecules of complex and three solvent molecules in the unit cell.

The molecular structures (Figures 2 – 4) of **2**, **10** and **13** reveal the typical piano-stool geometry seen for other η^5-Cp^x rhodium and iridium complexes.[30-33] The imino-sulfadoxine ligand chelates the metal in the expected *N,N'*-bidentate fashion. The bond angles and lengths (Table 1) show that the M-Cl bonds are slightly longer than the M-C or M-N bonds. The bond lengths between the metal and each carbon of the pentasubstituted cyclopentadienyl ring are all similar, as are the metal-centroid bond lengths in all three structures (ca. 1.50 Å). Rhodium complex **10** and iridium complex **13** are isomorphous and isostructural and their bond lengths and angles are almost identical, probably a consequence of the lanthanide contraction at the start of the 3rd transition series, resulting in Rh^{III} and Ir^{III} having similar sizes.

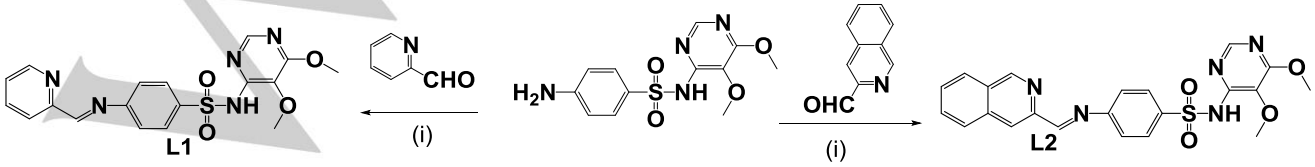

Scheme 1. Synthesis of pyridyl- and quinolyl-sulfadoxine ligands **L1** and **L2**. Reaction conditions: (i) microwave synthesis: MeOH/ 373 K/ 150 W/250 psi/ 5 min.

10.1002/chem.201801090

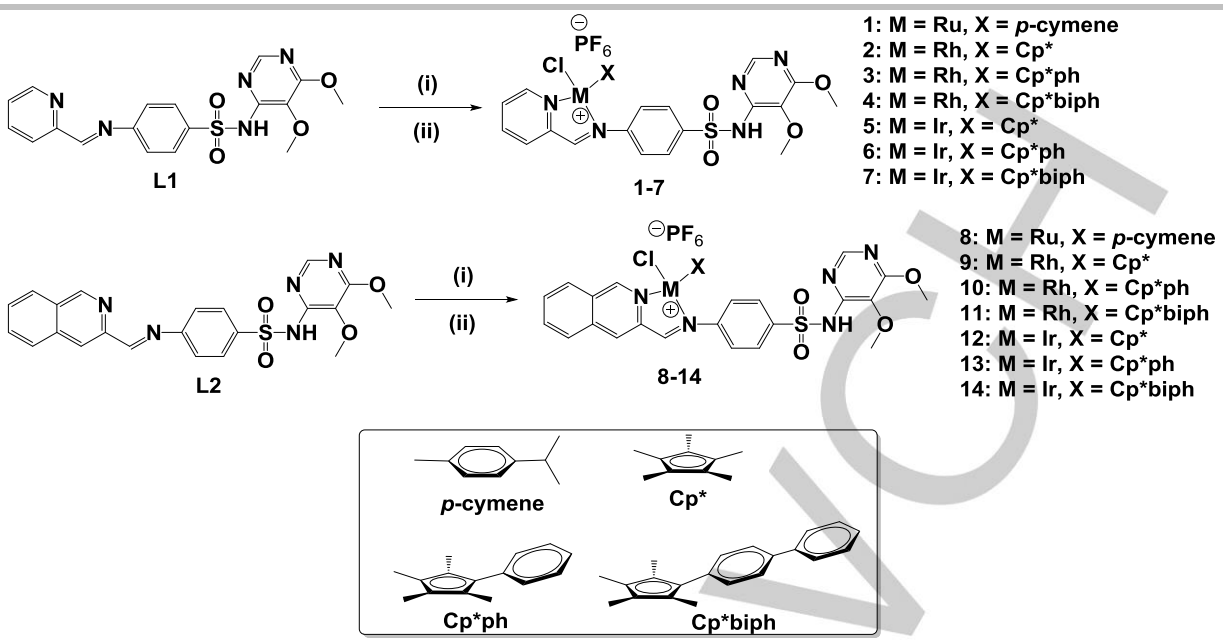

Scheme 2. Synthesis of pyridyl- and quinolyl-sulfadoxine PGM complexes (**1** -**14**). Reaction conditions: (i) $[MXCl_2]_2$/ RT/ MeOH; (ii) NH_4PF_6/ RT

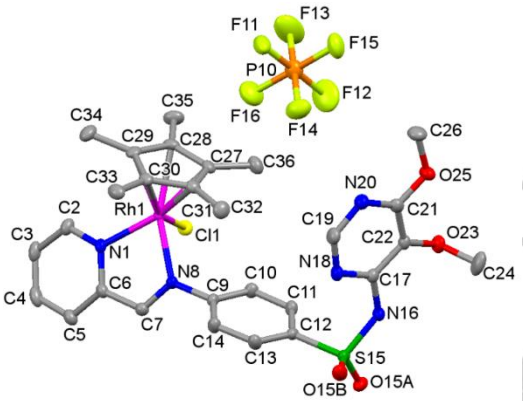

Figure 2. Molecular structure of rhodium Cp* complex **2** with atom labelling. Thermal ellipsoids are drawn at 50% probability level. All hydrogen atoms are omitted for clarity.

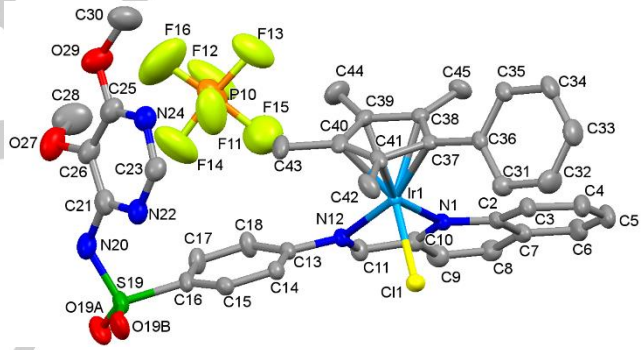

Figure 4. Molecular structure of iridium Cp^{*ph} complex **13** with atom labelling. Thermal ellipsoids are drawn at 50% probability level. All hydrogen and solvent atoms are omitted for clarity.

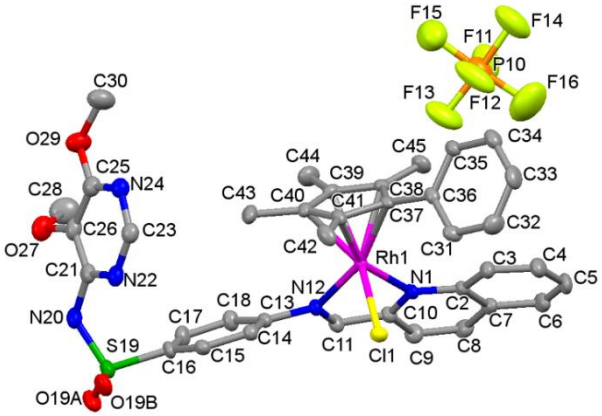

Figure 3. Molecular structure of rhodium Cp^{xph} complex **10** with atom labelling. Thermal ellipsoids are drawn at 50% probability level. All hydrogen and solvent atoms are omitted for clarity.

Aquation chemistry and relative hydrophobicity. Hydrolysis, substitution of the bound chloride by water thus producing a more reactive species, and hydrophobicity, which often determines the extent of cellular uptake, could be important factors in determining the activity of the members of this series of organometallic complexes.

The rate of hydrolysis of complexes **2**-**7** and **9**-**14** in 2.5% v/v DMSO in water at 37 ºC was monitored using UV-vis spectroscopy. Selected spectra are shown in Figure 5 and the change in absorbance at 325 nm over time was used to determine the half-lives ($t_{1/2}$, min) and pseudo first-order rate constants (k) (Table 2). All UV-vis spectra for complexes **2**-**7** and **9**-**11** are shown in the Supporting Information (Figures S1-S3). The formation of the aqua adduct was confirmed by ESI-MS (Supporting Information, Figures S4-S15).

10.1002/chem.201801090

FULL PAPER

Table 1. Selected bond lengths and angles for complexes **2**, **10**·1.5C_3H_6O and **13**·1.5C_3H_6O.

Complex 2			
Bond Lengths (Å)			
Rh1-Cl1	2.3980(6)	Rh1-C30	2.161(2)
Rh1-N1	2.1229(19)	Rh1-$C_{centroid}$[a]	1.492
Rh1-N8	2.1040(18)	S15-O15A	1.4274(18)
Rh1-C29	2.174(2)	S15-O15B	1.4225(19)
Rh1-C31	2.191(2)	N8-C7	1.282(3)
Rh1-C27	2.150(2)	N1-C2	1.336(3)
Rh1-C28	2.157(2)	N1-C6	1.356(3)
Bond Angles (º)			
$C_{centroid}$-Rh1-N8[a]	133.34	O15A-S15-N16	103.66(11)
$C_{centroid}$-Rh1-Cl1[a]	124.49	O15A-S15-C12	109.00(11)
$C_{centroid}$-Rh1-N1[a]	134.65	O15B-S15-O15A	119.53(11)
O15B-S15-C12	108.88(11)	O15B-S15-N16	109.56(11)
Complex 10			
Bond Lengths (Å)			
N1-Rh1	2.154(2)	Rh1-C41	2.174(3)
Rh1-Cl1	2.3935(7)	Rh1-$C_{centroid}$[a]	1.496
Rh1-N12	2.113(2)	C11-N12	1.287(3)
Rh1-C37	2.171(2)	N1-C2	1.372(3)
Rh1-C38	2.176(2)	N1-C10	1.333(3)
Rh1-C39	2.160(3)	O19A-S19	1.430(2)
Rh1-C40	2.182(2)	O19B-S19	1.430(2)
Bond Angles (º)			
$C_{centroid}$-Rh1-N12[a]	127.90	O19A-S19-O19B	119.54(15)
$C_{centroid}$-Rh1-Cl1[a]	127.35	O19A-S19-N20	104.07(14)
$C_{centroid}$-Rh1-N1[a]	132.14	O19B-S19-C16	108.49(14)
O19A-S19-C16	109.41(13)	O19B-S19-N20	110.01(14)
Complex 13			
Bond Lengths (Å)			
N1- Ir1	2.120(3)	Ir1-C41	2.173(3)
Ir1-Cl1	2.3989(9)	Ir1-$C_{centroid}$[a]	1.501
Ir1-N12	2.094(3)	C11-N12	1.380(4)
Ir1-C37	2.163(3)	N1-C2	1.341(4)
Ir1-C38	2.183(3)	N1-C10	1.333(3)
Ir1-C39	2.159(4)	O19A-S19	1.431(3)
Ir1-C40	2.186(4)	O19B-S19	1.415(3)
Bond Angles (º)			
$C_{centroid}$-Ir1-N12[a]	128.80	O19A-S19-O19B	119.8(2)
$C_{centroid}$-Ir1-Cl1[a]	127.75	O19A-S19-N20	103.8(2)
$C_{centroid}$-Ir1-N1[a]	132.62	O19B-S19-C16	108.87(18)
O19A-S19-C16	109.05(18)	O19B-S19-N20	110.4(2)

[a] Values calculated using Mercury 3.3 software

All of the complexes displayed changes in their spectra over time. As expected, the rate of hydrolysis decreases with an increase in the size of the Cp^x ligands in the order 1,2,3,4,5-pentamethyl > 2,3,4,5-tetramethyl-1-phenyl > 2,3,4,5-tetramethyl-1,1'-biphenyl. With respect to the metal, in the case of the pyridyl-sulfadoxine complexes **2**-**7**, the rhodium complexes undergo slower hydrolysis than the iridium derivatives. The opposite effect is observed for the quinolyl-sulfadoxine complexes (**9**-**14**).

The relative hydrophobicity of the iridium and rhodium complexes was determined by comparing their retention times on reverse-phase HPLC. Often the partition coefficient (LogP) is used as a measure of a compound's lipophilicity, and determined experimentally through partitioning between octanol and water.[34, 35] However, complexes **1**-**14** are relatively insoluble in water and octanol, and thus logP values could not be readily determined.

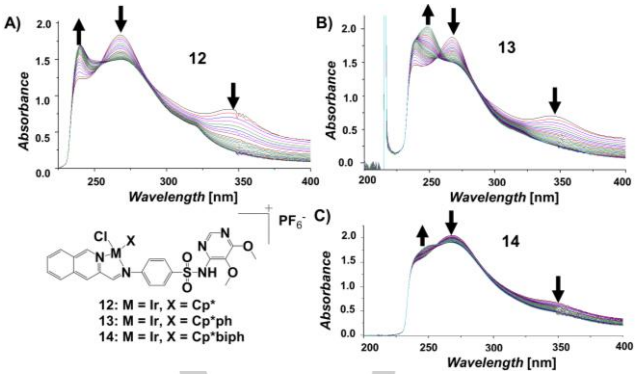

Figure 5. Time dependence of the UV-vis spectra for complexes **12**-**14** (50 µM) in 2.5% v/v DMSO in water. The isosbestic points are consistent with the conversion of the initial chlorido species to the aqua product. Scanning kinetics experiments were carried out at 37 ºC over 18 h.

Instead, a comparison of the hydrophobicity within each complex series can be made from the retention times of the chloride adducts of each complex. A similar approach has been used in other reports, e.g. Millett *et al*.[30] A 100 µM solution of each complex was prepared in 10 % CH_3CN/90 % 50 mM NaCl(aq). Each complex was eluted with a gradient of mobile phases: (A) 50 mM NaCl(aq) and (B) 50% CH_3CN:50% 50 mM NaCl(aq). The high salt concentration was necessary to suppress hydrolysis, thus giving only one peak in the HPLC trace for the chloride species. The mobile and stationary phases employed for RP-HPLC result in highly polar molecules eluting faster than less polar ones. The retention times (T_R) are directly proportional to hydrophobicity (Table 2). A clear trend is evident from the data. Complexes containing the quinolyl-ligand (**9-14**) are more hydrophobic than the pyridyl derivatives (**2-8**). Increasing the length of the Cp^x group also increases hydrophobicity and, in general, the rhodium complexes are slightly less hydrophilic than their iridium counterparts. A scatter plot correlating the rate of aquation and hydrophobicity (Figure 6) shows that within each series, the more hydrophobic complexes undergo water exchange of their chloride ligand at a much slower rate. The η^5-π-donor ligand influences this substitution in two ways, by increasing the hydrophobicity of the binding site and by steric effects.

Table 2. Half-lives and rates of hydrolysis of complexes **2**-**7** and **9**-**14** in 2.5% DMSO/97.5% water v/v and retention times of complexes on RP-HPLC.

Complex	$t_{1/2}$ (min) [a]	k (x 10^{-3} min^{-1}) [a]	Retention time (min)
2	12.9 (1.7)	53.9 (7.1)	6.61 ± 0.03
3	42.9 (4.8)	16.1 (1.8)	10.03 ± 0.01
4	182.9 (15.6)	3.79 (0.32)	13.93 ± 0.09
5	23.9 (1.8)	29.0 (2.2)	8.08 ± 0.04
6	95.7 (7.1)	7.27 (0.53)	11.27 ± 0.02
7	172.9 (8.1)	4.01 (0.19)	15.27 ± 0.18
9	5.35 (0.32)	129.5 (7.8)	9.27 ± 0.01
10	7.20 (0.21)	96.2 (2.8)	12.49 ± 0.01
11	90.2 (4.1)	7.68 (0.35)	16.19 ± 0.04
12	59.1 (1.6)	11.7 (0.3)	11.53 ± 0.14
13	81.3 (3.7)	8.53 (0.38)	13.73 ± 0.16
14	141.4 (3.7)	4.90 (0.13)	17.27 ± 0.13

[a] Half-lives $t_{1/2}$ and pseudo first order rate constants with standard error in parentheses.

10.1002/chem.201801090

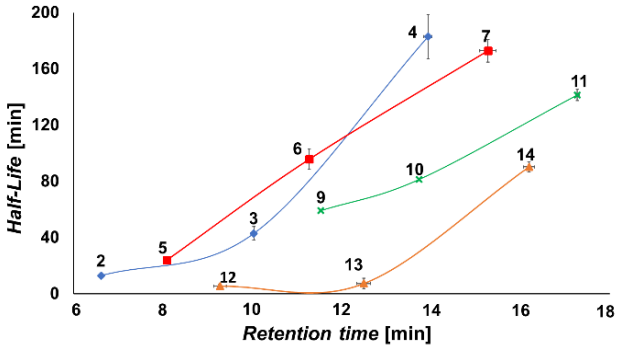

Figure 6. Plot of the half-life for aquation versus the RP-HPLC retention times of the chloride species as a measure of relative hydrophobicity. Legend: ● Rh pyridyliminosulfadoxine; ■ Ir pyridyliminosulfadoxine; ✖ Rh quinolylimino-sulfadoxine; ▲ Ir quinolyliminosulfadoxine.

***In vitro* Biological Activity.** Complexes **1**-**14** were screened for *in vitro* inhibitory activity against three *P. falciparum* strains (3D7 chloroquine-sensitive, Dd2 chloroquine-resistant and NF54 Late Stage Gametocytes (LSG), the *T. vaginalis* parasite strain G3 and *M. tuberculosis* H37Rv. To determine whether the complexes are selectively active as antimicrobial agents, they were also tested against the human ovarian cancer (A2780) and the human embryonic kidney (HEK293) cell lines. The data are shown in Tables 3 and 4. None of the complexes was toxic to the human embryonic kidney cell line, HEK293 up to the highest tested concentration of 80 µM demonstrating selectivity index values ranging from 4 to 320 for the Plasmodium parasite 3D7 in relation to HEK293 mammalian cells, and only three of the fourteen complexes (**7**, **11**, **14**) showed low to moderate inhibitory effects on the A2780 cell line, suggesting good antimicrobial selectivity. Overall, the rhodium and iridium complexes (**2**-**7** and **9**-**14**) displayed moderate to high potency as antimicrobial agents while their parent drug, sulfadoxine, is not active.

As antimalarial agents, the ruthenium complexes, **1** and **8**, were not active up to 20 µM. The rhodium complexes (**2**-**4** and **9**-**11**) were generally more active than the iridium derivatives (**5**-**7** and **12**-**14**) (Table 3 and Figure 7). Complexes **2**-**7** and **9**-**14** were active against LSG, while the drugs sulfadoxine (SFD), pyrimethamine (PY) and chloroquine (CQ) was inactive. This indicates that these complexes are active against both the asexual and sexual stages of the parasite life cycle, in contrast to the clinical drugs sulfadoxine, which is inactive for both asexual and sexual lifecycle stages. This is an important factor to note for future design.

Of note was the reduced activity of **2** and **9** against the chloroquine resistant strain Dd2, indicating potential parasite resistance. The ruthenium complexes (**1** and **8**) were not active, suggesting that the metallo-sulfadoxinyl derivatives of rhodium(III) and iridium(II) have greater potential for design as new antiplasmodial therapeutics. This is an interesting result; there are numerous reports of ruthenium-arene complexes displaying antiplasmodial activity.[4, 24, 36] It is possible that complexes **1** and **8** may be active at concentrations >20 µM. There are few published accounts where Rh^{III} and Ir^{III} analogues of Ru^{II} complexes were also tested for antiplasmodial activity in the same study.[15, 17, 37, 38] In most of these reported studies, the type of ligand used contained different pharmacophores compared to **1**-**14** and furthermore their intracellular targets are likely to be different, which may account for why the ruthenium-sulfadoxinyl complexes **1** and **8** are not active. This result further emphasises that it is not just the metal that is important for biological activity; but also, the choice of ligand, the oxidation state of the metal, and charge on the complex, all of which may play a role.

Table 3. IC_{50} values for complexes **1**-**14**, chloroquine (CQ), sulfadoxine (SFD) and pyrimethamine (PY) against the *Pf* strains 3D7, Dd2 and LSG, HEK293 cell line and the selectivity index (SI) for HEK293 vs 3D7 activities.

	Pf 3D7	*Pf* Dd2	*Pf* LSG NF54	HEK293	SI
Complex	**IC_{50} (µM)[a]**	**IC_{50} (µM) [a]**	**IC_{50} (µM) [a]**	**IC_{50} (µM) [b]**	**HEK293/ 3D7**
1	≈ 20	≈ 20	> 20	> 80	4
2	1.55 (0.613)	> 20	≈20	> 80	52
3	0.34 (0.06)	0.52 (0.18)	0.93 (0.36)	> 80	235
4	0.98 (0.14)	1.54 (0.12)	2.09 (0.047)	> 80	82
5	1.71 (0.05)	1.64 (0.10)	> 20	> 80	47
6	1.88 (0.15)	2.53 (0.97)	4.75 (0.04)	> 80	43
7	1.97 (0.13)	2.15 (0.31)	1.85 (0.22)	> 80	41
8	> 20	> 20	> 20	> 80	--
9	1.38 (0.43)	≈ 20	1.85 (0.08)	> 80	58
10	0.38 (0.24)	0.54 (0.19)	1.10 (0.09)	> 80	211
11	0.44 (0.09)	0.65 (0.03)	1.48 (0.39)	> 80	182
12	≈ 20	≈ 20	≈ 20	> 80	--
13	1.47 (0.04)	2.26 (0.37)	2.39 (0.32)	>80	54
14	0.25 (0.04)	0.17 (0.07)	1.23 (0.29)	> 80	320
CQ	0.012 (0.001)	0.06 (0.01)	> 20	> 40	4167
SFD	> 20	> 20	> 20	--	--
PY	0.005 (0.0001)	≈ 20	> 20	> 40	8000

[a] Average ± Standard deviation for 3 biological replicates performed in duplicate point given in parentheses; [b] HEK293 tested in duplicate point for 11 doses with the highest concentration tested being 80 µM.

Structure-activity trends reveal that the quinolylimino-sulfadoxine (**L2**) complexes are in general more active than their pyridyl-iminosulfadoxine (**L1**) counterparts. The complexes containing Cp^{*ph} or Cp^{*biph} (**3, 4, 10** and **11**) ligands show activities that are >1.5x higher than their unsubstituted Cp* ring derivatives (**2** and **9**). Of the pyridyl containing complexes, the $Cp^{*ph}Rh$ complex **3** displayed the highest activity against all three *Pf* strains (IC_{50} = 0.34 µM (3D7), 0.52 µM (Dd2) and 0.93 µM (LSG). Compared to the iridium derivative (**6**), complex **3** was 5.5 x more active against 3D7 (IC_{50} of **6** = 1.88 µM) and 5x more active against both Dd2 (IC_{50} of **6** = 2.53 µM) and LSG (IC_{50} of **6** = 4.75 µM). Interestingly, complex **3** had similar IC_{50} values to its quinolyl analogue **10** for all 3 *pf* assays (IC_{50} = 0.38 µM (3D7), 0.54 µM (Dd2) and 1.10 µM (LSG)), showing that for these two complexes, the extension of the aromatic imino group from pyridyl to quinolyl did not enhance its activity.

10.1002/chem.201801090

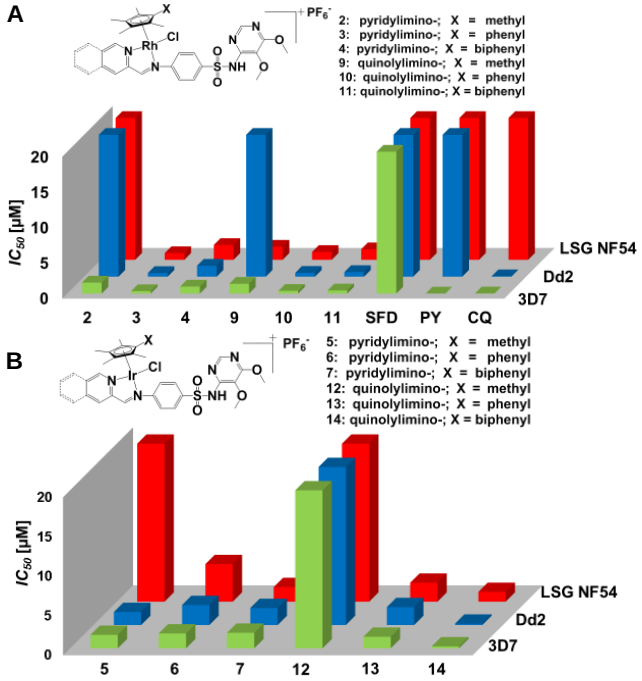

Figure 7. Graphical representations of the IC_{50} data for (A) drugs sulfadoxine (**SFD**), pyrimethamine (**PY**), chloroquine (**CQ**) and rhodium complexes **2-4**, **9-11**; and (B) iridium complexes **5-7**, **12-14**, in the 3 *P. falciparum* assays, 3D7 (green), Dd2 (blue) and LSG (red).

It was evident that for the Ir complexes **5-7**, there was no significant increase in activity towards 3D7 and Dd2 strains as the length of the cyclopentadienyl ligand increases, but there was an increase in antiplasmodial activity against the LSG strain (Table 2). The quinolyl iridium complexes, **12-14**, become more active with an increase in size of the cyclopentadienyl ligand. Out of all complexes tested, complex **14** displayed the highest activity in the asexual 3D7 and Dd2 assays (IC_{50} = 0.25 μM (3D7), 0.17 μM (Dd2)), perhaps a consequence of the combined effect of the quinoline and extended arene. Of note complex **14** also demonstrates greater than 320-fold selectivity for the 3D7 parasite in relation to HEK293 mammalian cells (Table 3). In fact, complexes **3**, **10**, **11** and **14** all have good starting selectivity indices for Plasmodium over HEK. The presence of the quinolylimino and tetramethylcyclopentadienylbiphenyl ligand makes complex **14** highly lipophilic which may result in increased uptake and a higher concentration of the drug reaching its target site. The complexes were slightly less active against the chloroquine-resistant strain Dd2, apart from complex **14** which was more active. Overall, complexes containing Rh are more potent than the Ir derivatives, although Ir complex **14** had the highest activity out of all the compounds tested (Figure 7).

In all 3 *Pf* assays, the pyridyl complexes (**3**, **4**, **6** and **7**) were less active that their quinolyl derivatives (**10**, **11**, **13** and **14**). The combination of the size of the aromatic imino group and the increase in extension of the pentasubstituted Cp^x ligand appears to influence activity beneficially. The structural importance of the Cp^x ligand and the aromatic imino group could be linked to the transport of these complexes to their intracellular targets. All potential antimalarials that target intracellular parasite functions need to cross three membranes by either lipid diffusion or flux through one or more transporters.[39] These membranes, in the order a drug would encounter them, are the host erythrocyte membrane (HEM), parasitophorous vacuolar membrane (PVM), and the parasite plasma membrane (PPM). Studies on antimalarial drug transport have found that an unusual plasmodial surface anion channel (PSAC) is induced in the HEM of infected cells to increase transport of essential ions and organic solutes.[39] This channel allows transport of solutes that are charged or uncharged with a molecular weight of greater than 600 Daltons, thus making it accessible to a variety of compounds.[40] Previous studies have shown that a number of potential drug leads utilize this channel to enter infected erythrocytes.[41-43] Complexes **2-7** and **9-14** are charged with molecular weights greater than 600 g/mol which may allow them to move through the HEM using this channel and also the PVM. Once in the erythrocyte cytosol, drugs need to traverse the PVM, which surrounds the parasite during its intracellular cycle. A large conductance ion channel exists at the PVM which mediates transport of both organic and inorganic cations and anions.[44, 45] Drug transport through the PPM is still not well understood with the general consensus being that most transporters at the PPM have highly controlled substrate specificity, so it is difficult to speculate on how complexes **2-7** and **9-14** traverse this membrane to enter the parasite. Nevertheless the positive charge on these complexes, their molecular weights and the increase in hydrophobic nature based on the imino group and the Cp^x ligand may allow increased transport through the first two membranes in the order of Cp^{*biph} > Cp^{*ph} > Cp* and quinolyl > pyridyl so that a greater concentration of complex can pass through the PPM by a yet-undiscovered mechanism to reach its site of action.

The clinical parent drug, sulfadoxine, displayed no antiplasmodial activity: demonstrating that conjugation to organometallic fragments enhances activity. Interestingly, the rhodium and iridium complexes (**3**, **4**, **6**, **7**, **9-11**, **13** and **14**) were all active in the LSG assay, while the clinical drugs chloroquine, sulfadoxine and pyrimethamine were inactive as expected. This is an important result for the design of new antimalarial metallo-drugs. Mature/late stage gametocytes of *Plasmodium* are responsible for parasite transmission from the mammalian host to the mosquito, thus propagating the spread of the disease.[46] Targeting LSG can lead to transmission-blocking; breaking the cycle of reinfection and reduce the prevalence of malaria cases. Complexes **3, 4, 6, 7, 9-11, 13** and **14** demonstrate that modification of the drug sulfadoxine with organometallic fragments beneficially alters its activity towards different stages of the malaria parasite's life cycle.

Against the trichomonas vaginalis strain **G3** (Table 4), all of the complexes displayed no or limited activity at 100 μM. The ruthenium complexes **1** and **8** had the lowest inhibitory effect on the parasite, 30% and 14%, respectively. For the rhodium complexes **2-4**, and **9-11**, and iridium complexes **5-7**, **12-14**, there was an increase in percent inhibition in the order: Cp^{*biph} > Cp^{*ph} > Cp^{*}. Similar to the antiplasmodial data, the best antitrichomonal activity was observed for the rhodium complexes, **3**, **4**, **10** and **11** (88, 92, 89 and 92% growth inhibition, respectively), but the iridium complex **14** (96%) displayed the best activity overall. The IC_{50} values showed that all these complexes exhibited 50% parasite inhibition at similar concentrations (IC_{50} = 15.2-18.1 μM).

10.1002/chem.201801090

Table 4. MIC_{50} in *M. tuberculosis*, IC_{50} in A2780 and % inhibition against *Tv* strain G3 for complexes **1**-**14**, sulfadoxine (SFD), pyrimethamine (PY), rifampicin (RFP) and isoniazid (INZ).

	M. tuberculosis	A2780	*Tv* G3	
Complex	**MIC_{50} (μM)**	**IC_{50} (μM)**	**% inhibition (x10²) (100 μM)[b]**	**IC_{50} (μM) [b]**
1	100	NA [a]	0.30 (0.09)	--
2	3.13-6.25	NA [a]	0.66 (0.02)	--
3	3.13	NA [a]	0.88 (0.02)	15.77 (0.95)
4	12.5	> 100	0.92 (0.02)	18.11 (0.91)
5	50	NA [a]	0.64 (0.10)	--
6	25	NA [a]	0.64 (0.08)	--
7	25	22.7 (0.4)	0.80 (0.02)	--
8	> 100	NA [a]	0.14 (0.13)	--
9	25	NA [a]	0.74 (0.12)	--
10	6.25	NA [a]	0.89 (0.02)	15.25 (0.92)
11	50	22.1 (0.3)	0.92 (0.03)	17.93 (0.90)
12	100	NA [a]	0.78 (0.01)	--
13	3.13	NA [a]	0.75 (0.08)	--
14	3.13	20.038 (0.004)	0.96 (0.01)	15.24 (0.89)
SFD	25-50	--	--	--
PY	NA [a]	--	--	--
RFP	0.003	--	--	--
INZ	0.3-0.6	--	--	--

[a] NA = not active, [b] R^2 squared value in given in parentheses.

The MIC_{50} values for complexes **1**-**14** were determined against *M. tuberculosis* H37Rv along with the drugs, sulfadoxine, pyrimethamine, rifampicin and isoniazid. Once again, the ruthenium(II) arene complexes were inactive. For the pyridylimino-sulfadoxine conjugates, the rhodium Cp^x complexes **2-4** (MIC_{50} = 3.13 - 6.25 μM, 3.13 μM and 12.5 μM, respectively) were more potent than the iridium Cp^x derivatives **5-7** (MIC_{50} = ~50 μM, 25 μM and 25 μM, respectively). This is in contrast to the quinolylimino-sulfadoxine complexes, where the iridium complexes **13** and **14** (MIC_{50} = 3.13 μM) are more active than the rhodium derivatives (MIC_{50} = 6.25 μM **10** and 50 μM **11**). Five of the fourteen complexes screened displayed notably good activities of < 6.25 μM, considerably more potent than the parent clinical drug sulfadoxine (MIC_{50} = 25-50 μM). All of the rhodium and iridium complexes were more active than pyrimethamine. At concentrations needed to induce 50% inhibition of the mycobacterial isolates, none of the complexes was as active as the antibiotics, rifampicin and isoniazid. There does not appear to be a straight forward structure-activity relationship for antimycobacterial activity. In the parasitic assays, the rhodium complexes showed better activities than the iridium derivatives, but contrastingly, the Rh pyridylimino complexes were more active than the Rh quinolylimino complexes in the *M. tuberculosis* assays. The opposite effect was noted for the iridium complexes. The most promising complexes for further development appear to be **2** (MIC_{50} = 3.13-6.25 μM), **3** (MIC_{50} = 3.13 μM), **13** (MIC_{50} = 3.13 μM) and **14** (MIC_{50} = 3.13 μM). Structurally, these four complexes have only the sulfadoxinyl fragment in common.

Plots of the half-lives for the aquation of the rhodium and iridium complexes against their *Pf* and *Tv* parasite activities (Figures S16A-D) showed that when comparing the activity within each series of complexes (**2-4, 5-7, 9-11** and **12-14**), in general, complexes that undergo water exchange at a slower rate displayed better activities as antiplasmodial and antitrichomonal agents. This suggested that as antiparasitics, the active species was the chloride complex and that rapid exchange of the chloride ligand with water rendered the complex inactive (shorter half-life). Replacement of a methyl group in the pentamethylcyclopentadienyl ligand with a phenyl or biphenyl substituent slowed down aquation of the complex which could allow the active chloride complex to remain intact until it reached its intracellular target. It is also important to note here, that the kinetics of aquation of the complexes were studied in salt free solution. Chloride present in biological media and in cells will affect the hydrolysis equilibria.

For the mycobacterial assay, there does not appear to be a correlation between the rate of aquation and bioactivity. Rhodium complex **3** (MIC_{50} = 3.13 μM) has similar activity to the iridium complexes **13** and **14** (MIC_{50} = 3.13 μM for both complexes) yet the latter have longer half-lives ($t_{1/2}$ = 42.9 min (**3**), 81.3 min (**13**) and 141.4 min (**14**). Complexes **5** and **12** were not active and displayed half-lives of 23.9 and 59.1 min, respectively. Clearly other factors such as the affinity for chloride and reactions with other intracellular components may also be involved in determining the antitubercular activity of these rhodium and iridium complexes. Figure 8 summarises the general activity trends observed for the organometallic sulfadoxine complexes. Activity is dependent on the metal, with ruthenium being inactive and rhodium generally the most active. Attachment of one or two phenyl rings to Cp* (to give Cp^{xph} or Cp^{xbiph} increases activity and increasing the size and planarity of the heteroaromatic ring of the imino group increases activity. Increasing the aromaticity of the sulfadoxinyl and cyclopentadienyl ligands renders the complex more lipophilic. However, this did not always result in an increase in activity (Figures S17A-D). In fact, the complexes that display 'intermediate' relative hydrophobicity (**3**, **6**, **10**) generally showed the best biological activity across all assays.

The high activity of the iridium complex **14** is attributable to the cooperative effect of the quinolylimino and Cp^{*biph} functionalities which could potentially facilitate transport across lipid membranes to reach intracellular parasite targets.

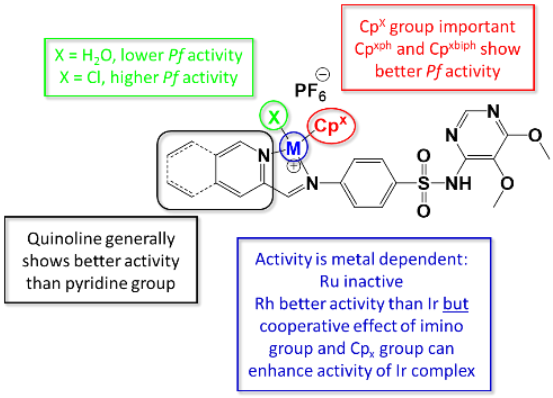

Figure 8. Features of structure-activity trends for complexes **1**-**14**.

10.1002/chem.201801090

Conclusions

Functionalisation of the drug sulfadoxine with pyridyl- or quinolyl-imino groups followed by organo-metallation yielded 14 new half-sandwich organo-ruthenium(II), -rhodium(III) and -iridium(III) complexes. In these complexes, the imino and pyridyl/quinolyl nitrogens provided an *N,N*-chelation site for the metal . Screening for *in vitro* biological activity against various parasite strains and *Mycobacterium tuberculosis* revealed that the ruthenium arene complexes were not active, and in general the rhodium Cp^x complexes were more active than their iridium counterparts, although iridium complex **14** displayed the best inhibitory activity out of all complexes screened. The parent drug, sulfadoxine, was not active in most of the assays, while the complexes were active; affirming the concept that derivatisation of drugs with organo-metallic fragments can beneficially affect bioactivity. Against the malaria parasite, most of the complexes displayed inhibitory activity in the sexual LSG assay, while the clinical drugs, pyrimethamine, sulfadoxine and chloroquine were inactive. This demonstrates that conjugation of organometallic groups to a drug can alter its biological target, as noted by others.[15, 21, 22, 47-56]
All the complexes studied contain a reactive metal-Cl bond which readily underwent aquation, although the rates varied widely, being slowest for the complexes with Cp^{xbiph} ligands with half-lives of >2 h (**4**, **7** and **14**), and fastest (minutes) for Cp* complexes (**2** and **9**). From this library, several complexes are promising for further development as antiparasitic and antitubercular agents. Work on structural modifications of **L1** and **L2,** as well as studies of the interactions of complexes **2**-**7** and **9**-**14** with potential biological targets, is currently underway.

Experimental Section

Chemicals and reagents. $RuCl_3{\cdot}3H_2O$, $RhCl_3{\cdot}3H_2O$, and $IrCl_3{\cdot}3H_2O$ were purchased from Precious Metals Online (PMO pty Ltd). All reagent solvents were obtained from Fisher Scientific and Sigma-Aldrich. Sulfadoxine (99 %), 2-pyridine carboxaldehyde, α-phellandrene and 1,2,3,4,5-pentamethylcyclopentadiene were purchased from Sigma Aldrich. 2-Quinoline carboxaldehyde was obtained from VWR Chemicals Limited. All reagents and chemicals were used as received. Deuterated solvents (CD_3CN, $CDCl_3$, MeOD-d_4, D_2O, DMSO-d_6) were purchased from Cambridge Isotopes Limited. Dichloro(*p*-cymene)ruthenium(II) dimer, dichloro(pentamethylcyclopentadienyl)rhodium(III) dimer, dichloro(pentamethylcyclopentadienyl)iridium(III) dimer, dichloro(4-(tetramethyl(biphenyl)cyclopentadienyl)iridium(III) dimer, dichloro(4-(tetramethyl(biphenyl)cyclopentadienyl)rhodium(III) dimer, dichloro(tetramethyl(phenyl)cyclopentadienyl)iridium(III) dimer and dichloro(tetramethyl(phenyl)cyclopentadienyl)rhodium (III) dimer were synthesised using a reported microwave method.[57]

Instrumentation. NMR data were acquired on either 400 MHz Bruker DRX-400, 500-MHz spectrometer Bruker DRX-500 or Varian 300 MHz spectrometers at ambient temperature unless otherwise stated. ^{1}H-NMR chemical shifts were internally referenced to residual protiated MeOD-d_4 (3.49 ppm), DMSO-d_6 (2.50 ppm), acetone-d_6 (2.05 ppm), or $CDCl_3$ (7.26 ppm). Elemental analysis was carried out on a CE-440 Exeter Elemental Analyzer by the Warwick Analytical Service. Electronic absorption spectroscopy spectra were recorded on Varian Cary 300 or Cary 300Bio UV-vis spectrometers using 1-cm path-length cuvettes. High resolution mass spectral data were obtained using methanolic solutions (50% MeOH in H_2O) on a Bruker Esquire 2000 instrument with electrospray as the ionization method. Microwave syntheses were carried out in a CEM Discover SP microwave reactor.

Purity measurements by HPLC were carried out using the Agilent 1200 system with a VDW and 100 µL loop. The column used was an Agilent Zorbax Eclipse Plus C18, 250 × 4.6 mm with a 5 µm pore size. The mobile phase was H_2O 0.1% TFA/MeCN 0.1% TFA at gradients of t = 0 min 10% B, t = 30 min 80% B, t = 40 min 80% B, t = 41 min 10% B, and t = 55 min 10% B over a 55 min period. The flow rate was 1 mL.min^{-1}, and the detection wavelength was set at 254 nm with the reference wavelength at either 360 or 510 nm. Samples were dissolved in 10% CH_3CN/90 % H_2O at ca. 100 µM. Sample injections were half the loop volume (50 µL) with needle washes of MeOH and H_2O between injections. It was assumed that all species in a sample have the same extinction coefficient at 254 nm. All peaks were manually integrated.

Synthesis of sulfadoxineimino ligands. Ligands **L1** and **L2** were prepared using the following procedures. Both compounds were isolated as crude solids and used for preparation of complexes **1**-**14** without further purification.

***N*-(5,6-dimethoxypyrimidin-4-yl)-4-((pyridin-2-ylmethylene)amino)-benzenesulfonamide (2-pyridyliminesulfadoxine)** (**L1**). Sulfadoxine (1.00 g, 3.22 mmol), 2-pyridine carboxaldehyde (0.345 g, 3.22 mmol) and anhydrous calcium oxide powder (0.050 g) were suspended in methanol (3 mL) in a microwave vial. The vial was sealed and placed in the microwave oven and the reaction was allowed to proceed, with stirring, under the following conditions: T = 373 K, *P* = 150 W, t = 5 min. Upon cooling to room temperature, the reaction mixture was diluted with methanol (5 mL) and filtered through celite on a medium-pore scintered funnel to remove the calcium oxide. The solvent of the filtrate was evaporated under reduced pressure and the crude residue redissolved in methanol (1 mL) and then passed through a small plug of florisil. After evaporation of the solvent, the oily solid isolated was washed with copious amounts of chloroform and dried to yield the crude product (**L1**) as a beige amorphous solid.

N-(5,6-dimethoxypyrimidin-4-yl)-4-((isoquinolin-3-ylmethylene)-amino)benzenesulfonamide (2-quinolyliminesulfdoxine) (**L2**). Sulfadoxine (1.00 g, 3.22 mmol), and 2-quinoline carboxaldehyde (0.506g, 3.2 mmol) were suspended in methanol (3 mL) in a microwave vial. The vial was sealed and placed in the microwave oven and the reaction was allowed to proceed, with stirring, under the following conditions: T = 373 K, *P* = 150 W, t = 5 min. Upon cooling to ambient temperature, the reaction mixture was diluted with methanol (5 mL) and filtered through celite on a medium-pore scintered funnel to remove the calcium oxide. The solvent from the filtrate was evaporated under reduced pressure and the crude residue redissolved in DCM (1 mL) and then passed through a small plug of florisil. After evaporation of the solvent, the oily solid isolated was dried under high vacuum to yield the product (**L2**) as a yellow crystalline solid.

Synthesis of Ru^{II}, Rh^{III} and Ir^{III} pyridyl- and quinolyl-sulfadoxine complexes.

General Synthetic Method. The ligand, either 2-pyridylimine-sulfadoxine (**L1**) or 2-quinolylimine-sulfadoxine (**L2**) (2 mol equiv.) was dissolved in methanol (15 mL) and the ruthenium, rhodium or iridium dimer (1 mol equiv.) was added. The reaction solution was stirred for 16 h at room temperature. Acetone (10 mL) was then added to redissolve any precipitate followed by ammonium hexafluorophosphate (2 mol equiv.). After stirring at room temperature for a further 2 h, the solution was filtered through celite and the volume was reduced to approximately 3 mL. The product was then precipitated from solution by addition of diethyl ether, isolated by vacuum filtration, washed with diethyl ether, and dried. Full characterization data of complexes **1**-**14** is given in the Supporting Information.

X-ray crystal structures

Complex 2. Single crystals of **2** were grown by slow evaporation of a solution of the complex in acteone. A suitable crystal was selected and mounted on a glass fibre with Fromblin oil on an Xcalibur Gemini diffractometer with a Ruby CCD area detector. The crystal was kept at 150(2) K during data collection. Using Olex2,[58] the structure was solved with the XS[59] structure solution program using Direct Methods and refined with the ShelXL[59] refinement package using Least Squares minimisation. The NH on N16 was located in a difference map. It was allowed to refine freely but given a U_{iso} 1.5 times the U_{equiv} of the parent nitrogen. It forms the short contacts listed in Table S2 in the Supporting Information .

Complex 10. Single crystals of **10** were grown from acetone/diethyl ether. A suitable crystal was selected and mounted on a glass fibre with Fromblin oil and placed on an Xcalibur Gemini diffractometer with a Ruby CCD area detector. The crystal was kept at 150(2) K during data collection. Using Olex2,[58] the structure was solved with the ShelXT[60] structure solution program using Direct Methods and refined with the XL[59] refinement package using Least Squares minimisation. The asymmetric unit contains the Rh complex, a PF_6 counter ion and one and a half molecules of acetone. Acetone C201-C203 lies very close to an inversion centre and was modeled at half occupied behind a PART -1 instruction. The NH was located on the sulphonamide nitrogen in a difference map. It was allowed to refine freely but given a Uiso 1.5 times the Uequiv of the parent nitrogen. It forms a short contact to a solvent acetone, Table S2.

Complex 13. Single crystals of **13** were grown from acetone/diethyl ether. A suitable crystal was selected and mounted on a glass fibre with Fromblin oil and placed on an Xcalibur Gemini diffractometer with a Ruby CCD area detector. The crystal was kept at 150(2) K during data collection. Using Olex2,[58] the structure was solved with the ShelXT[60] structure solution program using Direct Methods and refined with the ShelXL[59] refinement package using Least Squares minimisation. The asymmetric unit contains the iridium complex, a PF_6 counter ion and one and a half molecules of acetone. This occurs twice in the unit cell. The half-occupied molecule of acetone sits very close to an inversion centre and was refined behind a PARTS -1 instruction. The NH was located in a difference map on the pyrazine amine and allowed to refine freely but given thermal paramaters Uiso 1.5 times the Uequiv of the parent N20. It forms a short contact to the full occupied acetone oxygen, table S2. A SIMU restraint was used to give the thermal ellipsoids of the partially occupied acetone reasonable thermal parameters. This structure is isostructural (same structure) and isomorphic (same unit cell and space group) as **10.**

Hydrolysis studies. Hydrolysis of all complexes was monitored by UV–vis spectroscopy and the products verified by HR-ESI-MS. For UV–vis spectroscopy, the complexes were dissolved in DMSO and diluted with Milli-Q® purified H_2O to give 50 µM solutions with a final ratio of DMSO:H_2O of 2.5:97.5 v/v. The absorbance was recorded at several time intervals between 200-600 nm over 16 h at 310 K. Plots of the change in absorbance with time were computer-fitted to the pseudo-first-order rate equation, $A = C_0 + C_1e^{-kt}$ (where C_0 and C_1 are computer-fitted constants and A is the absorbance corresponding to time) using Origin version 9.1.0 to give the half-lives ($t_{1/2}$, min) and rate constants (k, min^{-1}).

Relative Hydrophobicity Studies. Relative hydrophobicity measurements by RP-HPLC were performed using the Agilent 1200 system with a variable wavelength detector (VWD) and 100 µL loop. The column used was an Agilent Zorbax Eclipse Plus C18, 150 × 4.6 mm with a 5 µm pore size. Mobile phase used was H_2O 50 mM NaCl/H_2O/MeCN 1:1 50 mM NaCl at gradients of t = 0 min, 20% B; t = 15 min, 100% B; t = 25 min 100% B; t = 27 min 20% B; and t = 35 min 20% B over a 35 min period. Flow rate was 1 $mL.min^{-1}$, and the detection wavelength was set at 254 nm with the reference wavelength at 360 nm. Sample injections were half the loop volume (50 µL) with needle washes of H_2O between injections. Samples were dissolved in 10% MeOH/90% H_2O in 50 mM NaCl at ca. 100 µM. Reported retention times (t_R) and standard deviations (SD) are from duplicates of triplicate measurements.

***M. tuberculosis* Resazurin Assay of Growth Inhibition.** The minimal inhibitory concentration (MIC) of compounds was determined using a modified version of the resazurin viability assay.[61] All compounds were initially prepared as 100 mM stocks in 100% DMSO and then adjusted to the required concentration in diluent (0.1% DMSO). Compounds (0.2− 100 µM) were added to wells in 2-fold dilutions and incubated for 7 days with *M. tuberculosis* H37Rv previously diluted to an OD_{600nm} of ca. 0.001. Resazurin (10 µL; 0.05% w/v; Sigma-Aldrich, Australia) was then added, and plates were incubated for 24 h at 310 K. The MIC was calculated by visual determination of colour change within wells or detection of fluorescence at 590 nm using a FLUOstar Omega microplate reader (BMG Labtech, Germany).

Evaluation of *in vitro* activity against *P. falciparum* asexual blood stages. Compounds were solubilized in DMSO to a final concentration of 5 mM. The stock compounds were then diluted further in DMSO to generate 3 doses per log dose response dilutions within 384-well polypropylene compound storage plates. The dose response dilution plates were then diluted 1 µL into 25 µL of sterile water and 5 µL transferred into 384-well imaging plates. The confocal image analysis assay is published in detail elsewhere.[62] In brief, the *P. falciparum* 3D7 and Dd2 strains were kept in continuous culture (RPMI supplemented with, 25 mM Hepes, 50 µg/mL hypoxanthine, 2.5 mg/mL Albumax II® plus 5% human serum) with sorbitol synchronization performed over two successive intra erythrocytic lifecycles to provide ring-stage parasites for use within the assays. On the day of assay, ring-stage parasite culture was adjusted to 2% parasitemia and 0.3% hematocrit and 45 µL of which was added to the compound-containing imaging plates. The assay plates were incubated for 72 h at 5% O_2, 5% CO_2 and 90% N_2. The plates were removed from incubation and allowed to equilibrate at room temperature prior to staining with 4',6-diamidino-2-phenylindole (DAPI). The imaging assay plates were then imaged on the Opera confocal imaging system. Using Accapella scripting software the number of classified parasites was determined for each assay well. Percent inhibition of parasite proliferation was calculated and normalized to assay control data of 0.4% DMSO and 5 µM Puromycin. Percent inhibition of parasite numbers (normalized to 5 µM puromycin) was plotted against log concentration of the compounds using a 4 parameter log dose, non-linear regression analysis, with sigmoidal dose response (variable slope) curve fit using Prizm 4.0. No constraints were placed on the top, bottom or Hill slope of the curve fit in the graphing software.

Evaluation of gametocytocidal *in vitro* activity. The assay is described elsewhere in detail.[63] In brief, the assay uses highly synchronous stage IV gametocytes induced from a transgenic NF54-$^{pfs16\text{-}Luc\text{-}GFP}$ parasite strain.[64] The gametocytes were harvested by magnetic isolation on day 8 and then added (45 µL of 10% gametocytes at 0.1% haematocrit) to the test compounds in 384 well imaging plates as described for the asexual blood stage *P. falciparum* assay above. Following the addition of the parasite to the test compounds, the plates were incubated for 72 h under reduced oxygen tension (5% CO_2, 5% O_2, 80% N_2). After incubation, Mitotracker Red CMH2XRos was added to the plates, which were then incubated overnight in standard conditions. After overnight incubation, the plates were imaged on the Opera confocal imaging system. Images for GFP and Mitotracker Red were overlaid and the number of elongated viable gametocytes per image determined using a script based on Acapella software developed for use with the Opera imaging system. The average Mitotracker Red fluorescence intensity was determined for objects greater than a determined size. Objects which were more than three times longer than they are wide were identified using the GFP images and are representative of gametocytes. Objects which were elongated and had Mitotracker Red fluorescent intensity above the cut-off limit were then identified as viable gametocytes. Using DMSO and 5 µM

puromycin as controls, the relative percent inhibition was calculated for the compounds. IC_{50} values were then calculated as described for the *P. falciparum* asexual blood stage assay described above.

Human embryonic kidney (HEK293) mammalian cell cytotoxicity. HEK293 cells were cultured in DMEM culture media supplemented with 10% Foetal Bovine Serum (FBS). The cells were harvested and dispensed into 384 well sterile black, clear base microtiter plates at 2000 cells/well (45 µL). The plates were left to settle and the cells attach overnight in a standard tissue culture incubator at 5% CO_2, 37ºC and 60% humidity. After overnight incubation, 5 µL of diluted compound (as described in the section, Evaluation of *in vitro* activity against *P. falciparum* asexual blood stages) was added to the cell containing plates and incubated for a further 72 h. After incubation the supernatant from the wells was removed and 40ul of 40 µM resazurin in DMEM media (FBS free) added to all wells. The plates were incubated for 6 h then measured for fluorescent intensity using the PerkinElmer Envision. The data were analysed as in the *Plasmodium falciparum* methods section.

Evaluation of *in vitro Trichomonas vaginalis* Growth Inhibition. Protozoal parasites were cultured for 24 h at 310 K. To perform the initial susceptibility screens on *T. vaginalis* (G3 genome strain), compounds were dissolved in DMSO to final concentrations of 100 µM; 5 µL aliquots of these suspensions were diluted in 5 mL of TYM diamond's media to obtain a final concentration of 100 µM. After 24 h, cells were counted using a hemacytometer. Cell counts were normalized to the DMSO controls, in order to allow direct comparison and averaging of the various trials. These data sets were then transformed using Prism Software, GraphPad, by taking the log of the drug concentrations for the trials, and inputting this transform into a log (inhibitor) versus response-variable slope regression option. Within this non-linear regression, constraints were set to force the maximum value (top) to 1 and the minimum value (bottom) to 0. The slope was left variable, and then determined through which regression was performed. The sample size consisted of 4 independent trials carried out on four different days (to account for possible variation in parasite culture). The assays were performed in 15 mL culture tubes, with both wildtype parasites and 0.1% DMSO-only treated parasites serving as control tubes to normalize for the effects of the solvent and in vitro conditions. After 24 h, cells were counted using a hemacytometer. The IC_{50} values for compounds **3, 4, 10, 11** and **14** were determined by running assays for increasing drug concentrations, 5–40 µM, and performing a regression analysis using Prism software from GraphPad. Calculated IC_{50} values of **3, 4, 10, 11** and **14** were then re-confirmed by testing again using the same assay described above.

Cancer Cell culture. A2780 ovarian cancer cells were obtained from the European Cell Culture Collection, grown as adherent monolayers in fully prepared Roswell Park Memorial Media (RPMI-1640 containing 10% FCS, 5% glutamine and 5% penn/strep) and were passaged using trypsin-EDTA when they had reached a 80% confluence. They were kept in a humidified 5% CO_2 atmosphere at 310K.

In vitro antiproliferative activity assay. Briefly, A2780 ovarian cancer cells were seeded in a 96-well plate at a density of 5000 cells/well. After 48 h of incubation in drug-free medium, cells were exposed to various concentrations of the metal complexes to be tested. A 24h drug exposure period was allowed, before removing the drug by suction, washing the cells with PBS and allowing three doubling times for recovery in drug-free medium. At the end of this period, cell survival was assessed using the sulforhodamine B assay as a measure of protein content in the treated cells compared to that of untreated controls. The experiments were carried out in duplicates of triplicates and their standard deviations were calculated.

Acknowledgements

We thank the National Research Foundation (NRF) of South Africa, ERC (grant 247450), EPSRC (grants EP/F034210/1 and EP/M027503/1), and Science City (AWM/ERDF) for support, and members of COST Action of CM1105 for stimulating discussions. KML and JL were supported by the Department of Biological Sciences at the University of the Pacific. LWC and CT were funded by the United States Department of Agriculture, Agricultural Research Service (National Program 108, Project #5325-42000-039-00D). This study was also supported by the Australian Research Council (LP120200557 award to V.M.A.). We thank the Australian Red Cross Blood Bank for the provision of fresh red blood cells, without which the *Plasmodium falciparum* research could not have been performed.

Keywords: Sulfonamides • antiparasitic • antitubercular • organometallic • transition metals •

References

[1] P.-Y. Shi, P. W. Smith, T. T. Diagana, *ACS Infect. Dis.* **2015**, *1*, 76-78.
[2] http://www.who.int/tb/publications/global_report/en/, Date accessed: 20/10/2017.
[3] http://www.who.int/malaria/publications/world-malaria-report-2016, Date Accessed: 20/10/2017.
[4] P. F. Salas, C. Herrmann, C. Orvig, *Chem. Rev.* **2013**, *113*, 3450-3492.
[5] World Health Organization: Guidelines for the Treatment of Malaria, 2nd ed.; WHO Press: Geneva, 2010.
[6] M. Enserink, *Science* **2010**, *328*, 844.
[7] World Health Organization. Global plan for artemisinin resistance containment (GPARC), WHO Press: Geneva, 2011.
[8] C. W. McNamara, M. C. S. Lee, C. S. Lim, S. H. Lim, J. Roland, A. Nagle, O. Simon, B. K. S. Yeung, A. K. Chatterjee, S. L. McCormack, M. J. Manary, A.-M. Zeeman, K. J. Dechering, T. R. S. Kumar, P. P. Henrich, K. Gagaring, M. Ibanez, N. Kato, K. L. Kuhen, C. Fischli, M. Rottmann, D. M. Plouffe, B. Bursulaya, S. Meister, L. Rameh, J. Trappe, D. Haasen, M. Timmerman, R. W. Sauerwein, R. Suwanarusk, B. Russell, L. Renia, F. Nosten, D. C. Tully, C. H. M. Kocken, R. J. Glynne, C. Bodenreider, D. A. Fidock, T. T. Diagana, E. A. Winzeler, *Nature* **2013**, *504*, 248-253.
[9] M. B. Jiménez-Díaz, D. Ebert, Y. Salinas, A. Pradhan, A. M. Lehane, M.-E. Myrand-Lapierre, K. G. O'Loughlin, D. M. Shackleford, M. Justino de Almeida, A. K. Carrillo, J. A. Clark, A. S. M. Dennis, J. Diep, X. Deng, S. Duffy, A. N. Endsley, G. Fedewa, W. A. Guiguemde, M. G. Gómez, G. Holbrook, J. Horst, C. C. Kim, J. Liu, M. C. S. Lee, A. Matheny, M. S. Martínez, G. Miller, A. Rodríguez-Alejandre, L. Sanz, M. Sigal, N. J. Spillman, P. D. Stein, Z. Wang, F. Zhu, D. Waterson, S. Knapp, A. Shelat, V. M. Avery, D. A. Fidock, F.-J. Gamo, S. A. Charman, J. C. Mirsalis, H. Ma, S. Ferrer, K. Kirk, I. Angulo-Barturen, D. E. Kyle, J. L. DeRisi, D. M. Floyd, R. K. Guy, *Proc. Natl. Acad. Sci. U.S.A* **2014**, *111*, E5455-E5462.
[10] U. Jungwirth, C. R. Kowol, B. K. Keppler, C. G. Hartinger, W. Berger, P. Heffeter, *Antioxid. Redox Signal.* **2011**, *15*, 1085-1127.
[11] P. Zhang, P. J. Sadler, *Eur. J. Inorg. Chem.* **2017**, *2017*, 1541-1548.
[12] I. Romero-Canelón, P. J. Sadler, *Proc. Natl. Acad. Sci. U.S.A* **2015**, *112*, 4187-4188.
[13] T. T. Ashburn, K. B. Thor, *Nat. Rev. Drug Discov.* **2004**, *3*, 673-683.
[14] Y. Y. Li, S. J. Jones, *Genome Med.* **2012**, *4*, 27.
[15] P. Chellan, K. M. Land, A. Shokar, A. Au, S. H. An, D. Taylor, P. J. Smith, T. Riedel, P. J. Dyson, K. Chibale, G. S. Smith, *Dalton Trans.* **2014**, *43*, 513-526.
[16] P. Chellan, K. M. Land, A. Shokar, A. Au, S. H. An, C. M. Clavel, P. J. Dyson, C. d. Kock, P. J. Smith, K. Chibale, G. S. Smith, *Organometallics* **2012**, *31*, 5791-5799.
[17] P. Chellan, K. M. Land, A. Shokar, A. Au, S. H. An, D. Taylor, P. J. Smith, K. Chibale, G. S. Smith, *Organometallics* **2013**, *32*, 4793-4804.
[18] P. F. Salas, C. Herrmann, J. F. Cawthray, C. Nimphius, A. Kenkel, J. Chen, C. de Kock, P. J. Smith, B. O. Patrick, M. J. Adam, C. Orvig, *J. Med. Chem.* **2013**, *56*, 1596-1613.
[19] C. L. Ferreira, C. B. Ewart, C. A. Barta, S. Little, V. Yardley, C. Martins, E. Polishchuk, P. J. Smith, J. R. Moss, M. Merkel, M. J. Adam, C. Orvig, *Inorg. Chem.* **2006**, *45*, 8414-8422.
[20] C. S. K. Rajapakse, A. Martínez, B. Naoulou, A. A. Jarzecki, L. Suárez, C. Deregnaucourt, V. Sinou, J. Schrével, E. Musi, G.

Ambrosini, G. K. Schwartz, R. A. Sánchez-Delgado, *Inorg. Chem.* **2009**, *48*, 1122-1131.
[21] D. Dive, C. Biot, *Curr. Top. Med. Chem.* **2014**, *14*, 1684-1692.
[22] F. Dubar, C. Slomianny, J. Khalife, D. Dive, H. Kalamou, Y. Guérardel, P. Grellier, C. Biot, *Angew. Chem. Int. Ed.* **2013**, *52*, 7690-7693.
[23] J. S. McCarthy, T. Rückle, E. Djeriou, C. Cantalloube, D. Ter-Minassian, M. Baker, P. O'Rourke, P. Griffin, L. Marquart, R. Hooft van Huijsduijnen, J. J. Möhrle, *Malar. J.* **2016**, *15*, 469.
[24] D. Gambino, L. Otero, *Inorg. Chim. Acta* **2012**, *393*, 103-114.
[25] M. L. Gatton, L. B. Martin, Q. Cheng, *Antimicrob. Agents Chemother.* **2004**, *48*, 2116-2123.
[26] A. R. Renslo, J. H. McKerrow, *Nat. Chem. Biol.* **2006**, *2*, 701-710.
[27] R. McKenna, C. Supuran, in *Carbonic Anhydrase: Mechanism, Regulation, Links to Disease, and Industrial Applications, Vol. 75* (Eds.: S. C. Frost, R. McKenna), Springer Netherlands, **2014**, pp. 291-323.
[28] Z. H. Chohan, H. A. Shad, M. H. Youssoufi, T. Ben Hadda, *Eur. J. Med. Chem.* **2010**, *45*, 2893-2901.
[29] Z. H. Chohan, M. Z. Hernandes, F. R. Sensato, D. R. M. Moreira, V. R. Alves Pereira, J. K. d. A. L. Neves, A. P. de Oliveira, B. C. de Oliveira, A. C. Lima Leite, *J. Enzyme Inhib. Med. Chem.* **2014**, *29*, 230-236.
[30] A. J. Millett, A. Habtemariam, I. Romero-Canelón, G. J. Clarkson, P. J. Sadler, *Organometallics* **2015**, *34*, 2683-2694.
[31] Z. Liu, I. Romero-Canelón, A. Habtemariam, G. J. Clarkson, P. J. Sadler, *Organometallics* **2014**, *33*, 5324-5333.
[32] P. Štarha, A. Habtemariam, I. Romero-Canelón, G. J. Clarkson, P. J. Sadler, *Inorg. Chem.* **2016**, *55*, 2324-2331.
[33] S. Thangavel, M. Paulpandi, H. B. Friedrich, K. Murugan, S. Kalva, A. A. Skelton, *J. Inorg. Biochem.* **2016**, *159*, 50-61.
[34] J. D. Bruijn, F. Busser, W. Seinen, J. Hermens, *Environ. Toxicol. Chem.* **1989**, *8*, 499-512.
[35] D. N. Brooke, A. J. Dobbs, N. Williams, *Ecotoxicol. Environ. Saf.* **1986**, *11*, 251-260.
[36] M. Navarro, W. Castro, C. Biot, *Organometallics* **2012**, *31*, 5715-5727.
[37] T. Stringer, R. Seldon, N. Liu, D. F. Warner, C. Tam, L. W. Cheng, K. M. Land, P. J. Smith, K. Chibale, G. S. Smith, *Dalton Transactions* **2017**, *46*, 9875-9885.
[38] Y. Li, C. de Kock, P. J. Smith, K. Chibale, G. S. Smith, *Organometallics* **2014**, *33*, 4345-4348.
[39] K. Basore, Y. Cheng, A. K. Kushwaha, S. T. Nguyen, S. A. Desai, *Front. Pharmacol.* **2015**, *6*.
[40] J. V. Cohn, A. Alkhalil, M. A. Wagner, T. Rajapandi, S. A. Desai, *Mol Biochem Parasitol* **2003**, *132*, 27-34.
[41] G. Lisk, M. Pain, M. Sellers, P. A. Gurnev, A. D. Pillai, S. M. Bezrukov, S. A. Desai, *Biochim. Biophys. Acta* **2010**, *1798*, 1679-1688.
[42] S. Dana, Prusty, D., Dhayal, D., Gupta, M.K. ,Dar, A., Sen, S., Mukhopadhyay, P., Adak, T. and Dhar, S.K., *ACS Chem. Biol.* **2014**, *9*, 2366-2373.
[43] A. M. W. Stead, P. G. Bray, I. G. Edwards, H. P. DeKoning, B. C. Elford, P. A. Stocks, S. A. Ward, *Mol Pharmacol.* **2001**, *59*, 1298.
[44] S. A. Desai, *Cell Microbiol.* **2012**, *14*, 1003-1009.
[45] S. A. Desai, S. M. Bezrukov, J. Zimmerberg, *Nature* **2000**, *406*, 1001-1005.
[46] T. Bousema, C. Drakeley, *Clin. Microbiol Rev.* **2011**, *24*, 377-410.
[47] E. Ekengard, L. Glans, I. Cassells, T. Fogeron, P. Govender, T. Stringer, P. Chellan, G. C. Lisensky, W. H. Hersh, I. Doverbratt, S. Lidin, C. de Kock, P. J. Smith, G. S. Smith, E. Nordlander, *Dalton Trans.* **2015**, *44*, 19314-19329.
[48] P. Beagley, M. A. L. Blackie, K. Chibale, C. Clarkson, J. R. Moss, P. J. Smith, *Journal of the Chemical Society, Dalton Transactions* **2002**, 4426-4433.
[49] R. Arancibia, A. H. Klahn, M. Lapier, J. D. Maya, A. Ibañez, M. T. Garland, S. Carrère-Kremer, L. Kremer, C. Biot, *J Organomet Chem* **2014**, *755*, 1-6.
[50] A. Singh, C. Biot, A. Viljoen, C. Dupont, L. Kremer, K. Kumar, V. Kumar, *Chem. Biol. Drug. Des.* **2017**, *89*, 856-861.
[51] A. Martínez, C. Deregnaucourt, V. Sinou, C. Latour, D. Roy, J. Schrével, R. A. Sánchez-Delgado, *Med Chem Res* **2017**, *26*, 473-483.
[52] M. I. F. Barbosa, R. S. Corrêa, K. M. de Oliveira, C. Rodrigues, J. Ellena, O. R. Nascimento, V. P. C. Rocha, F. R. Nonato, T. S. Macedo, J. M. Barbosa-Filho, M. B. P. Soares, A. A. Batista, *J Inorg Biochem* **2014**, *136*, 33-39.
[53] M. Adams, C. de Kock, P. J. Smith, K. M. Land, N. Liu, M. Hopper, A. Hsiao, A. R. Burgoyne, T. Stringer, M. Meyer, L. Wiesner, K. Chibale, G. S. Smith, *Dalton Trans.* **2015**, *44*, 2456-2468.
[54] N. Graf, S. J. Lippard, *Adv. Drug. Deliv. Rev.* **2012**, *64*, 993-1004.
[55] R. Arancibia, C. Quintana, C. Biot, M. E. Medina, S. Carrère-Kremer, L. Kremer, A. H. Klahn, *Inorg. Chem. Commun.* **2015**, *55*, 139-142.
[56] J. V. Mehta, S. B. Gajera, D. B. Raval, V. R. Thakkar, M. N. Patel, *MedChemComm* **2016**, *7*, 1617-1627.
[57] J. Tönnemann, J. Risse, Z. Grote, R. Scopelliti, K. Severin, *Eur. J. Inorg, Chem.* **2013**, *2013*, 4558-4562.
[58] O. V. Dolomanov, L. J. Bourhis, R. J. Gildea, J. A. K. Howard, H. Puschmann, *J. Applied Cryst.* **2009**, *42*, 339-341.
[59] G. Sheldrick, *Acta Crys. A* **2008**, *64*, 112-122.
[60] G. Sheldrick, *Acta Crys. A* **2015**, *71*, 3-8.
[61] S. Ellis, D. S. Kalinowski, L. Leotta, M. L. H. Huang, P. Jelfs, V. Sintchenko, D. R. Richardson, J. A. Triccas, *Mol. Pharmacol.* **2014**, *85*, 269-278.
[62] S. Duffy, V. M. Avery, *Am. J. Trop. Med. Hyg.* **2012**, *86*, 84-92.
[63] S. Duffy, V. M. Avery, *Malar. J.* **2013**, *12*, 408.
[64] M. J. Delves, U. Straschil, A. Ruecker, C. Miguel-Blanco, S. Marques, A. C. Dufour, J. Baum, R. E. Sinden, *Nat. Protocols* **2016**, *11*, 1668-1680.

10.1002/chem.201801090

WILEY-VCH

Entry for the Table of Contents

FULL PAPER

Novel arene Ru^{II}, and cyclopentadienyl Rh^{III} and Ir^{III} complexes containing a chelated pyridylimino- or quinolylimino ligand functionalized with the antimalarial drug sulfadoxine exhibit potent antiplasmodial activity, as well as activity in gametocyte assays, and against *Mycobacterium tuberculosis* whereas sulfadoxine itself was inactive.

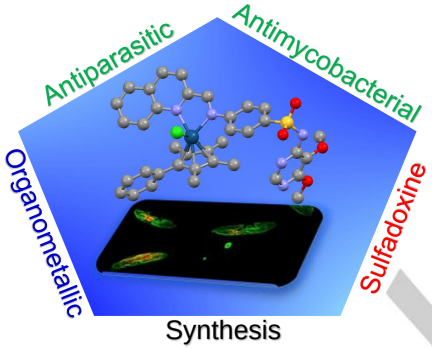

Prinessa Chellan, Vicky M Avery, Sandra Duffy, James A. Triccas, Gayathri Nagalingam, Christina Tam, Luisa W. Cheng, Jenny Liu, Kirkwood M. Land, Guy J. Clarkson, Isolda Romero-Canelón, Peter J. Sadler

Page No. – Page No.

Organometallic conjugates of the drug sulfadoxine for combatting antimicrobial resistance